Particles I

Access the latest eBook →

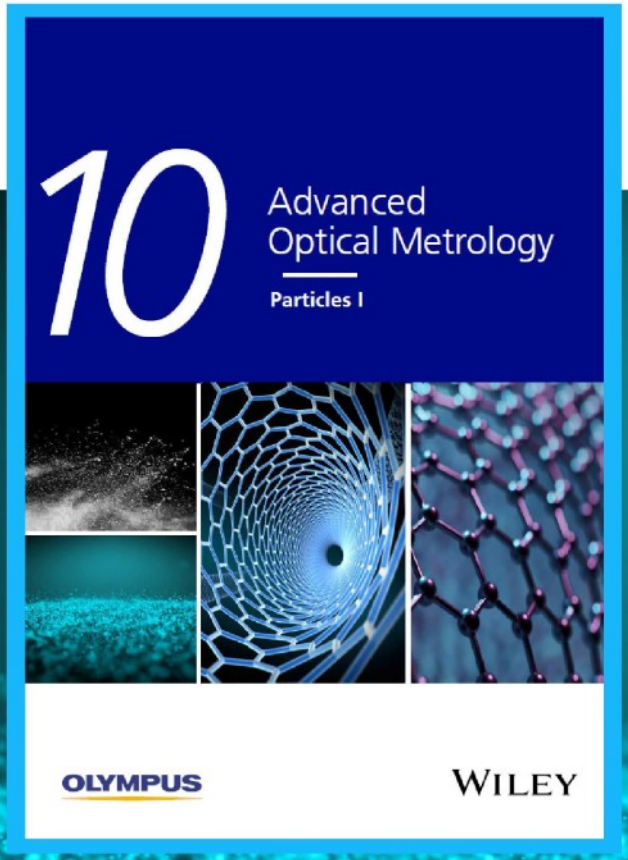

Particles: Unique Properties, Uncountable Applications

Read the latest eBook and better your knowledge with highlights from the recent studies on the design and characterization of micro- and nanoparticles for different application areas.

Access Now

This eBook is sponsored by

OLYMPUS

WILEY

ADVANCED FUNCTIONAL MATERIALS
www.afm-journal.de

Non-Classical Electrostriction in Hydrated Acceptor Doped $BaZrO_3$: Proton Trapping and Dopant Size Effect

*Evgeniy Makagon, Olga Kraynis, Rotraut Merkle, Joachim Maier, and Igor Lubomirsky**

Point defects such as oxygen vacancies and protonic interstitials are not only essential for ionic conductivity in oxides since they also affect the mechanical and electromechanical properties. These properties of nominally dry and hydrated proton-conducting $BaZr_{0.85}M_{0.15}O_{2.925+\delta}H_{2\delta}$ (M = Al, Ga, Sc, In, Y, Eu) ceramics are investigated. Doping decreases Young's modulus with increasing ionic radii difference between the dopant and the host. Nominally dry samples show consistently higher Young's moduli than hydrated samples. All samples exhibit large non-classical electrostriction, with a negative electrostriction coefficient $M_{33}<0$. M_{33} shows saturation with the field and a non-ideal Debye relaxation with frequency. The low-frequency M_{33} value for both dry and hydrated samples shows a similar dependence on dopant radius as Young's modulus. For the hydrated samples, the relaxation frequency increases by a factor >100 in the series Ga-Y, emphasizing the importance of proton trapping, with Y-doped samples having minimal trapping energy. This coincides with the fact that the saturation strain for Y-doped samples is also the smallest. In light of these findings, it is concluded that the present data give strong evidence for the existence of defect-related elastic dipoles in acceptor doped barium zirconate and that the non-classical electrostriction originates in their reorientation under electric field.

1. Introduction

Electrostriction is a second-order electromechanical response. Mathematically, electrostriction strain coefficients (M_{ijkl}) represent a fourth-rank tensor linking the strain components (u_{ij}) with the component of the applied electric field (E):[1]

$$u_{ij} = M_{ijkl} \cdot E_k \cdot E_l \quad (1)$$

E. Makagon, O. Kraynis, I. Lubomirsky
Department of Materials and Interfaces
Weizmann Institute of Science
Rehovot 7610001, Israel
E-mail: Igor.Lubomirsky@weizmann.ac.il
R. Merkle, J. Maier
Max Planck Institute for Solid State Research
Heisenbergstr. 1 , 70569 Stuttgart, Germany
The ORCID identification number(s) for the author(s) of this article can be found under https://doi.org/10.1002/adfm.202104188.

DOI: 10.1002/adfm.202104188

a relation which simplifies to $u_{ii} = M_{iiii} E_i^2$ for a uniaxial case. Since symmetry does not impose limitations on the existence of fourth-rank tensor-described properties, some electrostriction response exists in all materials, irrespective of their structure. In 1997, Newnham et al.[1] suggested an empirical law applicable to a wide range of materials, including polymers, classical dielectrics, ferroelectrics, and relaxors. According to this empirical law, the hydrostatic electrostriction coefficient (Q) scales, in power ≈0.6, with the ratio of the material elastic compliance (S) to its dielectric susceptibility (ε). Since $M_{xxxx} \approx Q\,(1 - 2\nu)\,(\varepsilon_0\,\varepsilon)^2$ (ν is the Poisson's ratio in x-direction), M_{xxxx} scales with $S^{0.6}(\varepsilon_0\,\varepsilon)^{1.4}$ (see Equation S1 in Section S1, Supporting Information, and ref. [2]). Thus, to exhibit large strain electrostriction coefficients a material must either have a very large dielectric constant, as for instance the commercial ferroelectric relaxor (2/3) $PbMg_{0.33}Nb_{0.66}O_3 - (1/3)PbTiO_3$ ($\varepsilon > 10\,000$, $S \approx 10^{11}$ Pa^{-1}, $M_{33} \approx 10^{-16}$ m^2 V^{-2}), or a large elastic compliance, as realized for polymers ($\varepsilon < 10$, $S > 10^{10}$ Pa^{-1}, $M_{33} \approx 10^{-18}$ m^2 V^{-2}).[1]

Recent works[2–9] report that in well-studied oxygen ion conductors, such as Gd, Sm, Ca-doped ceria, and $Bi_7Nb_{2-x}Y_xO_{15.5-x}$ (x = 0.4–1.6), the electrostriction effect is much larger than expected from classical (Newnham's) electrostriction (measured $M_{33} \approx 10^{-18} - 10^{-16}$ m^2 V^{-2}, expected $M_{33} \approx 10^{-20} - 10^{-19}$ m^2 V^{-2}). The nature of this non-classical electrostriction is still under investigation. The leading hypothesis is that in these materials, the dopants introduced to induce oxygen vacancies resulting in ionic conductivity also induce highly polarizable elastic dipoles.[10] An external electric field causes these dipoles to reorient, leading to local and macroscopic strain. According to this "host-guest" hypothesis of non-classical electrostriction,[2–6,11] the dielectric ($\varepsilon < 80$) and the elastic ($S < 10^{11}$ Pa^{-1}) properties are largely defined by the host, whilst the electrostriction originates from the guest-induced (defect-induced) elastic dipoles. While this hypothesis is still under development, the fact that both doped ceria and (Y,Nb)-stabilized bismuth oxide are strongly anelastic, clearly proves that these materials contain elastic dipoles. Moreover, the fact that undoped ceria does not show strong anelasticity supports the hypothesis that elastic dipoles are induced by the dopants. Both doped ceria and (Y,Nb)-stabilized bismuth oxide have a fluorite structure with dopant-induced mobile oxygen vacancies, which

poses the of question whether non-classical electrostriction is limited to materials of a defective fluorite structure.

The current work reports on the electromechanical response of $BaM_{0.15}Zr_{0.85}O_{2.925+\delta}H_{2\delta}$ (M = Al, Ga, Sc, In, Y, Eu) perovskite ceramics. These materials are extensively studied because upon hydration, $\delta > 0$, they exhibit considerable protonic conductivity[12] making them very attractive, for example, for protonic ceramic fuel cells. For this study, these materials are of specific interest because of two aspects:

1. $BaM_xZr_{1-x}O_{3-x/2+\delta}H_{2\delta}$ has a cubic perovskite structure, which acquires oxygen vacancies upon B-site acceptor doping (Al, Ga, Sc, In, Y, Eu) for charge compensation:

$$M_2O_3 + 2Zr_{Zr}^{x} + O_O^{x} \rightleftharpoons 2M'_{Zr} + V_O^{\cdot\cdot} + 2ZrO_2 \quad (2)$$

Examining the nominally dry state of these materials gives a glimpse at the electromechanical response of oxygen vacancies in lattices other than fluorite.

2. Upon hydration the vacancies are filled with hydroxyl groups (protonic defects):[12]

$$H_2O + V_O^{\cdot\cdot} + O_O^{x} \rightleftharpoons 2OH_O^{\cdot} \quad (3)$$

replacing oxygen vacancies as the main point defect, thus, providing a possibility to compare the electromechanical response of two different point defects in the same lattice.

Previous computational and experimental studies on the influence of point defects on the mechanical properties of doped $BaZrO_3$ (BZO),[13,14] showed a decrease of the elastic moduli upon doping because of chemical bond weakening due to oxygen vacancy formation. Even though hydration fills the oxygen vacancies, it further decreases elastic moduli because proton incorporation significantly weakens the oxygen-cation bonds.[14] The size of the dopant was shown to be a strong factor that influences the mechanical properties,[14] as larger dopants cause larger deformation and expand the lattice parameter. The dopant size strongly affects proton mobility as well. A large body of experimental and theoretical data[15–24] indicates that at low temperatures only a fraction of the protons in hydrated perovskite oxides ($BaZrO_3$, $SrZrO_3$, $SrCeO_3$) are mobile, while the majority of the protons are trapped by acceptor dopants, due to, predominantly, columbic attraction and/or elastic interactions. The electrostatic part of the trapping energy is expected to decrease with the increasing ionic radius of the dopant. From density functional theory (DFT) calculations, trapping energies in the range of 0.49 eV for Ga^{3+} decreasing to 0.28 eV for Sc^{3+} have been obtained[20] which follows the trend of stronger trapping for smaller dopants (for these dopants the protons are trapped in the first coordination sphere around the acceptor). For Y^{3+}, protons have comparable energy when bound to O in the first and second coordination shell around Y^{3+},[20] these positions are stabilized relative to > 4.5 Å separation by about 0.3 eV.[13,25] While the trapping energies for protons in the first sphere around In^{3+} and the second sphere around Y^{3+} are comparable, in the latter case the proton has more low-energy sites accessible without the need for de-trapping.[23] Other factors which may affect the protons-dopant interaction such as the material's dielectric constant (for screening of the electrostatic attraction) and elastic properties are related to the host material and should hardly vary with the dopant.

In the trapped state, protons undergo precession around the acceptor dopant, because the proton transfer barriers are low but de-trapping would require a perceptible additional energy of 0.2–0.5 eV.[20,22,25] Thus they are expected to behave as an elastic dipole capable of reorientation and contributing to electromechanical response.

The data on the electrostriction in $BaM_{0.15}Zr_{0.85}O_{2.925+\delta}H_{2\delta}$ (M = Al, Ga, Sc, In, Y, Eu, $\delta < 0.075$) ceramics presented in this work testify on two important accounts: i) The investigated materials exhibit non-classical electrostriction ($M_{33} \approx 10^{-17} - 10^{-16}$ m^2 V^{-2}), which expands the range of materials exhibiting this effect. ii) The electrostriction relaxation frequency in hydrated samples rapidly increases with the radii of the dopant, supporting the hypothesis suggesting that the acceptor-trapped protons form the elastic dipoles responsible for electrostriction.

2. Results and Discussion

All peaks in the X-ray diffraction (XRD) patterns of Al, Ga, Sc, In, Y and Eu doped BZO samples were identified as belonging to a perovskite phase (Figure S1a,b, Section S2, Supporting Information). Scanning electron microscope (SEM) images of the top surface of the samples demonstrated dense structure with no visible open porosity (Figure S2a–f, Supporting Information). Grain size was shown to be 1.5–3.5 μm with non-significant dependency on dopant size (Figure S3, Supporting Information). Dopants with ionic radii smaller than the host[26] decrease the lattice parameter (**Figure 1**a) due to the combined effect of the small dopant and oxygen vacancy formation-induced contraction. Dopants with ionic radii larger than that of the host cause lattice expansion because the effect of the large dopant radius dominates over vacancy-induced lattice contraction. The ionic radii of Eu^{3+} is large enough with respect to Zr^{4+} (33% mismatch) to cause dopant distribution between both B-sites and A-sites. This is evident from the Eu luminescence spectra containing features attributed to 12-fold coordination (Figure S4a, Supporting Information). As a result, the Eu-doped BZO has a smaller lattice parameter than the Y-doped one.[27–29] Eu^{3+} on A-site compensates for its presence on B-site (Figure S4b, Supporting Information), making oxygen vacancy formation less favorable (See Section S3, Supporting Information). Since the exact B/A distribution cannot be determined reliably, the degree of hydration is also less reliable for Eu-doped samples. The presence of Eu^{3+} on A-site makes Eu-doped samples less relevant for the discussion of mechanical and electrostrictive properties, indicating that Y is the largest among the here investigated dopants that can be reliably introduced exclusively on the B-site.

According to our previous report,[14] the ceramics preparation and hydration processes used here result in [OH]/x ≈13 ± 3% for nominally dry samples, and ≈64 ± 5% for hydrated samples. Using these values and the calculated lattice parameters, the relative density of all samples was 95–98% of the theoretical (Figure S5, Section S4, Supporting Information), with the uncertainty mostly originating from limited precision of the degree of hydration. Sample density exceeding 95% of the theoretical one suffices for reliable ultrasound pulse time of flight (USTOF) measurements of elastic moduli.

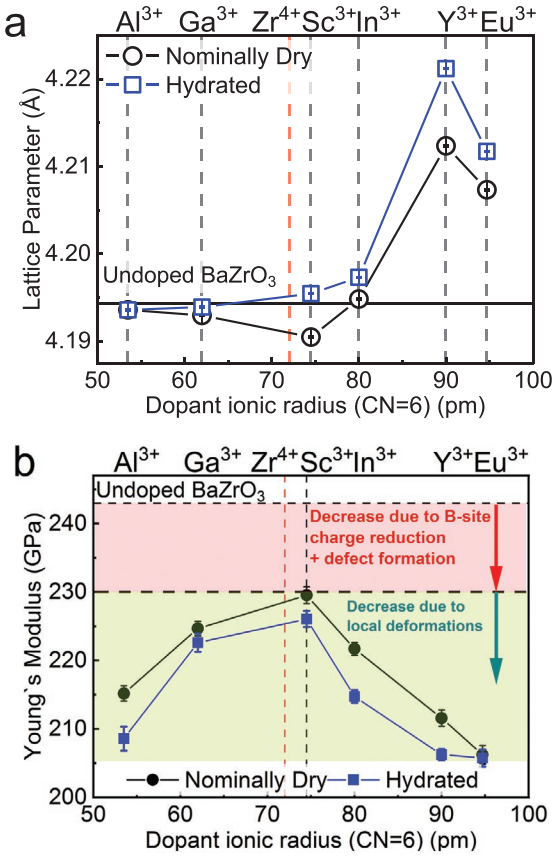

Figure 1. Structural characterization of $BaZr_{0.85}M_{0.15}O_{2.925+\delta}H_{2\delta}$ M = Al, Ga, Sc, In, Y, Eu in the nominally dry and hydrated states: a) Lattice parameters as a function of dopant ionic radius. Undoped lattice parameter was taken from Levin et al.[39] b) Young's modulus as a function of dopant ionic radius. Undoped Young's modulus was taken from Yamanaka et al.[40]

The dependence of Young's modulus on dopant radius exhibits two regions (Figure 1b) for both nominally dry and hydrated samples. 1) In the series Al^{3+}, Ga^{3+} and Sc^{3+},Young's modulus increases. 2) in the series Sc^{3+}, In^{3+}, Y^{3+} and Eu^{3+}, it decreases. Thus Sc-doping results in the smallest decrease in the Young's modulus (230 ± 1 GPa for nominally dry and 226 ± 1 for hydrated) with respect to undoped BZO (242 ± 1 GPa). Similar to previous studies,[13,14] Young's modulus of the nominally dry samples is consistently slightly higher than for hydrated samples. There are four notes to make regarding these results.

a) Sc^{3+} has the smallest size mismatch with respect to the host (Zr^{4+}), ≈3%, which implies that the minimum in the decrease of Young's modulus corresponds to the minimum in lattice distortions.
b) The decrease in Young's modulus comes from four contributions:[13] i) Decrease in the effective number of bonds due to vacancy formation. ii) Decrease in the charge of the B-site cation for dopants, and anion charge by substitution of oxide by hydroxide ions. iii) Lattice distortions due to the size mismatch between a dopant and the host. iv) Decrease or expansion of the overall lattice parameter. The first two contributions are similar for all dopants except Eu, which directly implies that (iii) and (iv) contributions are the smallest for Sc-doped sample (Figure 1b). The Sc^{3+} ionic radius is the closest to that of Zr^{4+} (only 3% mismatch) and the changes to the lattice parameter due to Sc-doping are very small. Therefore, one should expect that even though contributions (iii) and (iv) do exist for Sc, they are much smaller than (i) and (ii). In these terms, the difference in Young's modulus between the Sc-doped samples and undoped BZO is close to the sum of the first two contributions. Consequently, the difference between Young's modulus of the Sc-doped samples and the Al, Ga, In and Y-doped samples is the contribution of the lattice distortions caused by the respective dopants. Y doping leads to a significant lattice parameter expansion (Figure 1a), which also significantly contributes to the modulus decrease(Figure 1b).[13]
c) The data in Figure 1b suggest that the dopants with similar size mismatch with respect to the host cause a similar decrease in Young's modulus, irrespective of whether the mismatch is positive or negative. For instance, Al-doped sample: mismatch ≈−26%, Y_{dry} = 215 ± 1 GPa, $Y_{hydrated}$ = 209 ± 2 GPa; and Y-doped sample mismatch ≈+25%, Y_{dry} = 212 ± 1 GPa, $Y_{hydrated}$ = 206 ± 1 GPa.
d) No difference in Young's modulus between nominally dry and hydrated Eu-doped samples was observed. This is consistent with the finding that at least some Eu^{3+} occupies A-sites, which impedes the formation of oxygen vacancies and decreases hydration[28] (See Equation S2 in Section S3, Supporting Information). This makes the Eu-doped samples less informative for elucidating the link between doping, hydration, and elastic moduli.

Only second-order electromechanical response, that is, electrostriction was detected (**Figure 2**a and Figure S6a in Section S5, Supporting Information). All samples contracted in the direction of the applied field ($M_{33} < 0$). This is similar to the observations for acceptor doped ceria and bismuth oxide,[2,6,11] both of which have a fluorite structure, but it is contrary to the most conventional electrostrictors (with perovskite or other structure). The samples exhibited strain saturation with an electric field, and electromechanical relaxation with frequency. Below the saturation strain, the absolute value $|M_{33}|$ can be approximated by a non-ideal Debye relaxation function (Figure 2b,c):

$$M_{33}(f) = \frac{M_{33}^{0}}{\sqrt{(\tau \cdot f)^{2+\alpha} + 1}} + M_{33}^{\infty} \quad (4)$$

where M_{33}^{0} and M_{33}^{∞} are the values of the strain electrostriction coefficient below and above the relaxation respectively, τ is the relaxation time ($f_r = 1/\tau$ is the relaxation frequency) and α is the non-ideality factor ($\alpha = 0$ corresponds to a single relaxation time). The magnitude of the response, $|M_{33}^{0}|$, the relaxation frequency, f_r, and the saturation strain have a profoundly different dependence on dopant ionic radii.

2.1. $|M_{33}^{0}|$ as a Function of Dopant Radii

Below the saturation strain and relaxation frequency, the values of $|M_{33}^{0}|$ have a narrow distribution ≈ $(1 - 7) \cdot 10^{-16}$ m^2 V^{-2}

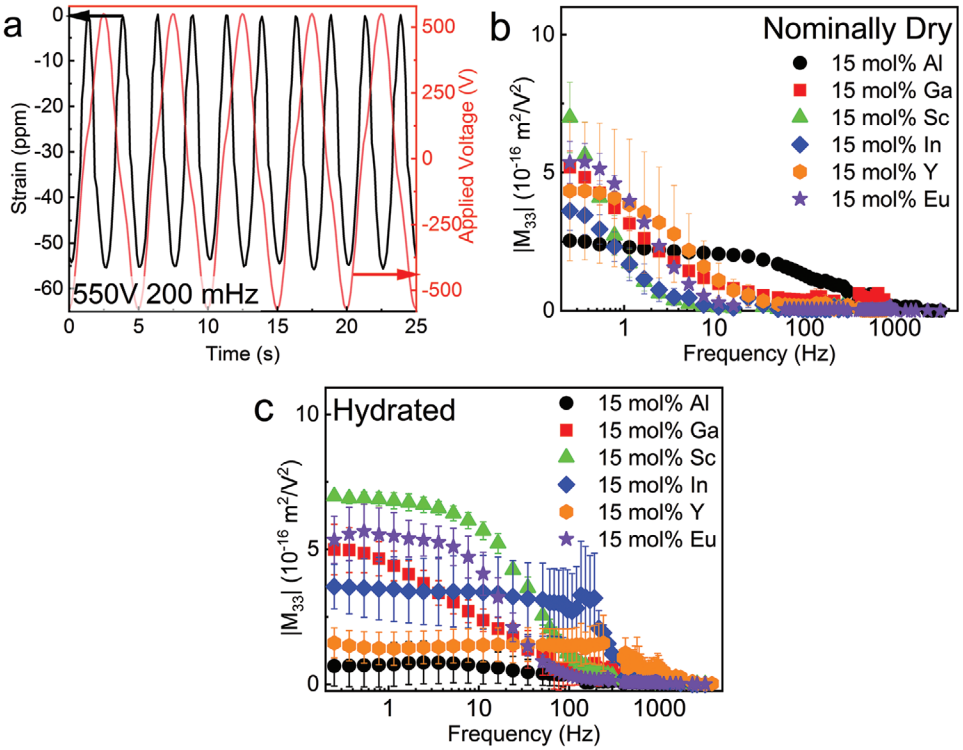

Figure 2. Electromechanical characterization of $BaZr_{0.85}M_{0.15}O_{2.925+\delta}H_{2\delta}$ M = Al, Ga, Sc, In, Y, Eu: a) Sinusoidal strain generation time trace in hydrated $BaZr_{0.85}Sc_{0.15}O_{2.925+\delta}H_{2\delta}$ in response to 550V. Two cycles of contraction are clearly visible for each cycle of applied voltage. b) Average strain electrostriction coefficient as a function of the frequency of applied electric field for nominally dry samples. c) Average strain electrostriction coefficient as a function of the frequency of applied electric field for hydrated samples.

(**Figure 3**a). These values exceed those expected from Newnham's scaling law[1] by as much as 3–4 orders of magnitude (expected $\approx 10^{-19}$ m^2 V^{-2}). Above the relaxation frequency, $|M_{33}^0|$ drops by a factor of up to 100 to 10^{-18}–10^{-17} m^2 V^{-2}, which is still well above classical (Newnham's) electrostriction (expected $\approx 10^{-20}$ m^2 V^{-2}) (See Figure S6b,c in Section S5, Supporting Information). Taking into account that the elastic dipoles responsible for the electrostriction below the relaxation frequency ($|M_{33}^0|$-range) do not contribute above the relaxation (i.e., in M_{33}^∞-range), one has to conclude that each dopant induces at least two types of local distortions, forming two types of elastic dipoles. Assuming that at sufficiently high-frequency Newnham's scaling law is obeyed, non-classical electrostriction above the relaxation frequency implies that the relaxation time of the second type of elastic dipoles is above the measurement range (3 kHz). This is similar to the observations reported for Gd- and Sm- doped ceria.[6,11,30]

Even though $|M_{33}^0|$ varies relatively little between the different samples, one can clearly see two trends. Similar to Young's modulus (Figure 1b), $|M_{33}^0|$ increases in the line Al^{3+}, Ga^{3+}, Sc^{3+} and decreases in the line Sc^{3+}, In^{3+}, Y^{3+}, Eu^{3+} (Figure 3a). Sc doped samples show the largest $|M_{33}^0|$, even though it has the largest Young's modulus, which is contrary to the expectations based on Newnham's scaling law predicting lower electrostriction for materials with larger Young's modulus (See Equation S1 in Section S1, Supporting Information). Within the accuracy of the measurement, $|M_{33}^0|$ is similar for the hydrated and the nominally dry samples except for the case of Al.

2.2. Relaxation Frequency (f_r) as a Function of Dopant Radii

All hydrated samples (except Al-doped) have a higher relaxation frequency than their nominally dry counterparts (Figure 3b). This is in line with the suggestion that the elastic dipoles in these samples originate from different defects, oxygen vacancies, and hydroxide ions on oxide sites (protonic defects). The latter is slightly smaller than oxide ions,[31] and of anisotropic character. The barriers for reorientation of protons (while attached to the same oxygen) and for transfer to a neighboring oxygen are significantly smaller than oxygen vacancy migration barriers,[12] which in particular at low temperature (25 °C) drastically increases the jump rates. Therefore, the protonic defects are expected to respond faster. Furthermore, the majority of the $V_O^{\cdot\cdot}$ introduced by the acceptor doping is consumed by the hydration in pure steam according to Equation (3).

The relaxation frequencies of 0.3–2 Hz observed for dry samples (Figure 3b) are similar to that of oxygen vacancies in a fluorite structure.[6,11,30] The nominally dry samples have a very weak dependence of f_r on ionic radii in the line Ga^{3+}, Sc^{3+}, In^{3+} and Y^{3+}, with less than a decade between the highest (Y^{3+}) and the lowest (Sc^{3+}) sample. In the hydrated samples, the f_r increases by about three orders of magnitude in the line Ga^{3+}, Sc^{3+}, In^{3+} and Y^{3+}, which clearly indicates that the OH_O in Y-doped BZO is the most labile defect in all samples. This dependence clearly correlates with ionic conductivity, which, similar to f_r increases drastically from Ga^{3+} to Y^{3+} doping.[32] This trend in f_r supports the hypothesis that the protons in doped BZO strongly interact

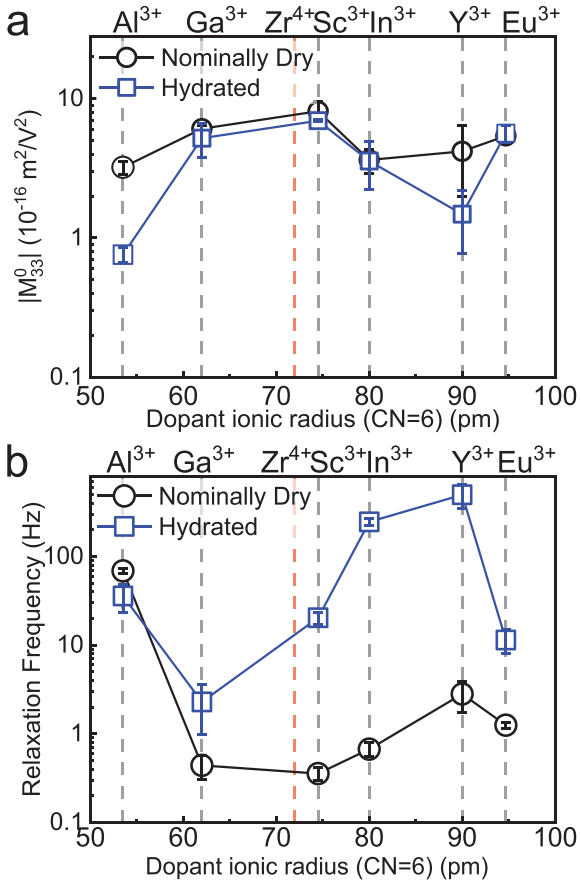

Figure 3. Results of the fitting of the data shown are in Figure 2 to Equation (4). An average of at least 3 independent measurements was taken. a) Low-frequency strain electrostriction coefficient (M_{33}^0) as a function of dopant ionic radius. b) Relaxation frequency as a function of dopant ionic radius.

with the dopant ion (proton trapping), otherwise, f_r, would not depend on the dopant ionic radius.

This agrees with previous studies in zirconates,[20,32] stannates,[33] and cerates[34] reporting a minimum of proton-dopant trapping energy for dopants with a radius significantly larger than the host cation and close to that of Y^{3+}.[32] Eu-doped samples do not follow the trend, probably because Eu^{3+} occupies both A and B sites with different effects on elastic dipoles, making the interpretation of their behavior very complex. For samples doped with the very small Al^{3+} the f_r values are close for nominally dry and hydrated samples and do not follow the trend observed for Ga^{3+}, Sc^{3+}, In^{3+} and Y^{3+}, indicating that the local distortions in these samples differ strongly from those with other dopants.

The electrostriction relaxation frequencies show a very good match with the dielectric relaxation frequencies deduced from the impedance spectroscopy measurements (Figure S7 and Figure S8, Section S6, Supporting Information). However, interpretation of the impedance spectra is difficult because it is dominated by blocking grain boundaries. For further details, see Section S6, Supporting Information.

2.3. Strain Saturation with Electric Field

Strain saturation with electric field was observed for all samples (Figure S9a,b, Section S7, Supporting Information). It can be approximated with equal fit quality as a Langevin curve or as an exponential decay, yielding similar values for saturation strain u_{sat} and saturation field E_{sat} (**Figure 4**a,b):

$$u\left(E^2\right) = u_{sat}\left(1 - e^{-\frac{E^2}{E_{sat}^2}}\right) \quad (5)$$

For Ga, Sc, In and Y samples, the saturation field has a very narrow spread of 0.5–1 MV m^{-1} without any detectable differences between nominally dry and the hydrated samples. The saturation strain, however, follows the same trend as a function of dopant radius as Young's modulus and $|M_{33}^0|$ (Figure 1b and Figure 3a): in the line Al^{3+}, Ga^{3+} and Sc^{3+}, the saturation strain increases by a factor of two, and then, in the line of Sc^{3+}, In^{3+} and Y^{3+}, it decreases by a factor of ten. The saturation strain for the hydrated Al, Ga and Sc samples is larger than for their nominally dry counterparts. However, for In and Y-doped samples, hydration leads to a dramatic decrease in the saturation strain, and for Y-doped samples u_{sat} is particularly small.

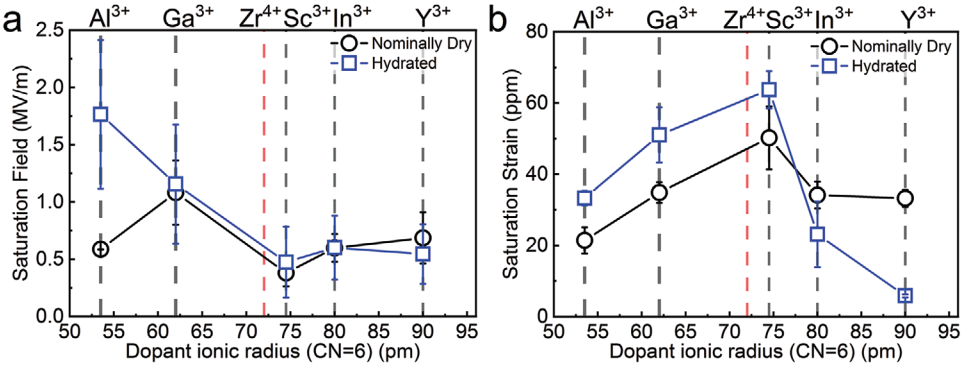

Figure 4. a) Saturation field and b) Saturation strain as a function of dopant ionic radius for $BaZr_{0.85}M_{0.15}O_{2.925+\delta}H_{2\delta}$ M = Al, Ga, Sc, In, Y in the nominally dry and hydrated states. Saturation parameters were deduced from averaging the fitting results to Equation (5) of 2–3 independent measurements.

The saturation strain is the sum of the local strain resulting from the reorientation of the elastic dipoles. Since the concentration of the elastic dipoles is roughly the same in all samples, the differences in the saturation strain indicate the difference in the strength of these dipoles (strength of an elastic dipole is the change in the local strain resulting from its reorientation times the volume of the regions where this strain takes place).[35] The relatively small spread in u_{sat} for the nominally dry samples indicates that the properties of the elastic dipoles related to oxygen vacancies depend only weakly on the nature of the dopant. This fact agrees with the observation that the electrostriction relaxation frequency for the nominally dry samples depends weakly on the dopant radii (Figure 3b).

For the hydrated samples, the local elastic dipole is expected to be related, to the movement of a proton around an acceptor-dopant at which it is trapped. The dipole strength, in this case, is correlated with the ability of the proton to move between oxygen ions coordinated to the same acceptor ion, rather than to move to a different position in the lattice. Therefore, the decrease in the saturation strain in the line Sc^{3+}, In^{3+} and Y^{3+} indicates a drastic decrease in the strength of the elastic dipoles. It can be partially attributed to the decrease in the proton trapping energy,[32] which may affect both the probability of the proton staying in the vicinity of the dopant and the average distance between the dopant and the trapped proton.

For dopants smaller than the Sc^{3+}, lattice contraction obstructs elastic dipole reorientation. In this respect, the maximum u_{sat} values observed in Sc-doped samples coincide with the fact that these samples have the smallest local distortions. Following the hypothesis that the proton-related elastic dipoles in Y-doped BZO are the weakest among all dopants, we have measured the electrostriction response in hydrated Y-doped samples in the concentration range 5–20 mol% (**Figure 5**). It was found that f_r does not depend on the dopant concentration. This implies that the elastic dipoles in these samples do not interact even though they are located at an average distance of $1/\sqrt[3]{0.6\,\delta} \approx 2.2$ unit cells. This clearly indicates that the elastic dipoles are weak, which agrees with the fact that the saturation strain for Y-doped samples is the smallest. For this case, the presence of protons (which are distributed in the first and second coordination shell around Y) does not lead to large macroscopic effects.

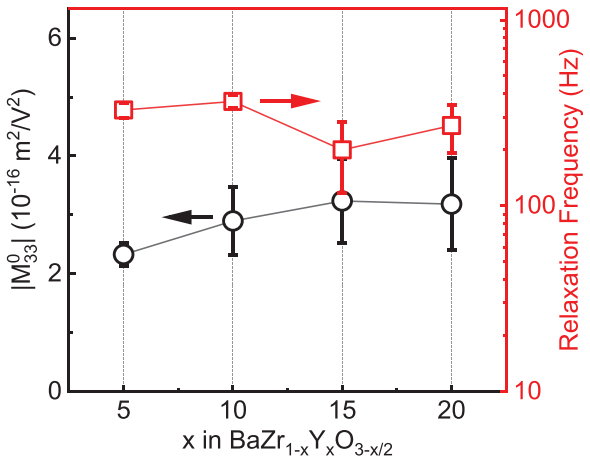

Figure 5. Average low-frequency strain electrostriction coefficient (M^0_{33}) and relaxation frequency as a function of dopant concentration in $BaZr_{1-x}Y_xO_{3-x/2}$ in the hydrated state. M^0_{33} and relaxation frequency ($1/\tau$) was deduced from averaging the fitting results to Equation (4) of 3–4 independent measurements.

2.4. DFT Calculations

To gain some microscopic understanding of the distortions associated with the dopant-proton interaction, we exploit DFT calculations which were conducted for the investigation of elastic properties.[13] In the first coordination shell, the presence of a proton stretches the O-(B-cation) distances by more than 4% (**Figure 6**a, Figure S11a, Supporting Information, for Sc). This leads to anisotropic distortions of the supercells, such that the B-(OH) direction is largest or second-largest, and the O—H direction the shortest (see section S9 and S10, Supporting Information). Thus, locally the lattice becomes non-centrosymmetric. Therefore, an external electric field applied to such a structure inevitably alters the local strain prompting the elastic dipoles to reorient to accommodate this change. Moreover, the distortions extend to more than one unit cell and involve noticeable displacement of more than ten oxygen ions and cations (Figure 6b,c, Figure S11b, Supporting Information, for Sc). One has to point out that even if the proton remains close to a dopant but changes bonding from one oxygen ion to a neighboring one, it would still induce displacements of many other oxygen ions. This prediction agrees with the relatively low electromechanical relaxation frequencies even for the case of Y-doping, for which the trapping energy is the lowest. The dependence of the relaxation frequency and the saturation strain on dopant ionic radii and the related trapping energy is complex because it depends on two factors with opposite trends (Figure 4). An increase in the host-dopant mismatch increases distortions of the lattice, impeding any additional field-induced rearrangement of the atoms. On the other hand, the host-dopant mismatch decreases the elastic moduli (Figure 1b), making the rearrangement easier. Therefore, a detailed understanding of this issue requires further investigations by more extended atomistic modeling. This is challenging because one has to deal with several contributions to the electric dipole (O—H, Y'-(OH_O), local lattice distortions), and also with the fact that a treatment beyond the static picture might be required since the rotation of the proton around the oxygen to which it is bound is fast even at room temperature. Also for reduced or acceptor doped ceria—another material with complex defect chemistry and remarkable electrostriction properties (in absence of protons)—so far only a qualitative relation between elastic dipoles obtained by DFT and measured electrostriction coefficient is reported.[36]

3. Conclusions

Our experimental findings provide the following insights into the mechanical and electromechanical properties of the

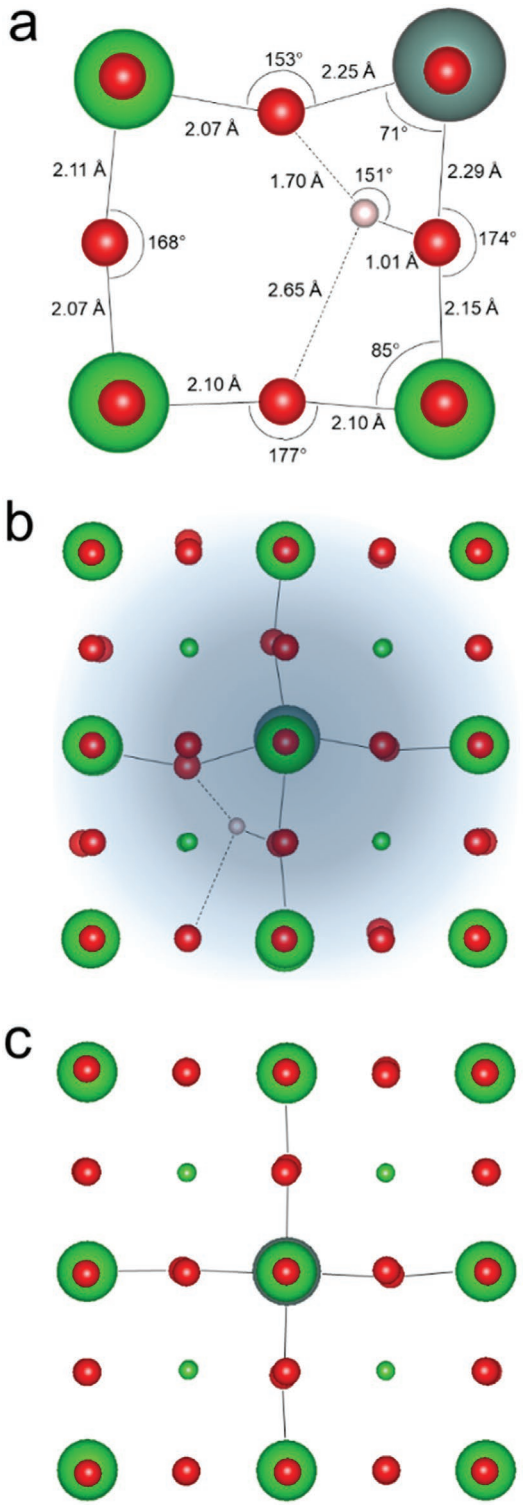

Figure 6. Local distortions induced by proton incorporation, taken from DFT calculations of $3 \times 3 \times 3$ supercells in ref. [13] (O red, Zr green, Y gray, H light gray, Ba small green spheres). a) Environment of Y with a proton in first coordination shell, showing that oxygen ions undergo large displacements to compensate for the formation of a short covalent O—H bond and two longer O···H hydrogen bonds. b) View of Y in $3 \times 3 \times 3$ supercell along (100) direction, showing that even for the case of Y, in which the proton trapping energy is lowest, the distortions extend to more than one unit cell. c) Less distortions around Y when the proton is at a large distance.

acceptor doped BZO, all of which can be interpreted in terms of local distortions behaving as elastic dipoles.

1. Young's modulus and the electrostriction saturation strain reach their maxima in Sc-doped samples, as Sc^{3+} is the closest to Zr^{4+} in size. This strongly suggests that both properties are largely defined by the magnitude of the local lattice distortions.
2. The introduction of oxygen vacancies and local charge reduction at B-site of the lattice in 15 mol%-doped samples accounts for a moderate decrease in Young's modulus. The host-dopant size mismatch may result in a softening of the lattice exceeding the first two contributions.
3. The hypothesis of local distortions and local elastic dipoles agrees with the data on the electrostriction behavior. The relaxation frequencies for nominally dry samples have a relatively narrow distribution, while for hydrated samples it increases by three orders of magnitude in the series Ga^{3+}, Sc^{3+}, In^{3+} and Y^{3+}, which correlates with the data on proton trapping. The data on the saturation strain also shows that the least bound protons generate the least strain (Y-doped samples). However, the full dependence is more complex because saturation strain depends on a multitude of factors. Small saturation strain in Y-doped samples implies that the elastic dipoles in them are weak and, therefore, do not interact with each other. This explains the fact that the saturation field and the relaxation frequency for Y-doped hydrated samples do not depend on the concentration in the 5–20 mol% range.
4. According to DFT calculations, proton incorporation causes highly asymmetric local distortions extending for more than one unit cell and involving at least ten oxygen ions and cations on both A and B sites. This fully supports the hypothesis on the presence of an elastic dipole coupled to an electric dipole.

Taken together these findings strongly support the existence of polarizable elastic dipoles in acceptor doped BZO. The interaction of protons with dopants (trapping) play an important role by i) preventing excessive long-range conductivity, ii) allowing for localized reorientations, and iii) affecting frequency of these reorientations and the resulting magnitude of local distortions. Thus, for the presently investigated materials, the nature of the non-classical electrostriction is, at least partially, understood.

4. Experimental Section

$BaM_xZr_{1-x}O_{3-x/2+\delta}H_{2\delta}$ samples with M = Al, Ga, Sc, In, Eu, x = 0.15 and Y with $0.05 < x < 0.2$ were prepared using a solid-state reactive sintering method which employs a tiny NiO addition to form a small amount of a (Ba, Ni, Acc)O_x transient liquid phase.[37] The corresponding amounts of $BaCO_3$ (Alfa Aesar), ZrO_2 (Tosoh TZ0), Al_2O_3, Ga_2O_3, Sc_2O_3, In_2O_3, Y_2O_3 and Eu_2O_3 (Alfa Aesar), were weighted and dry ball milled (Friatec zirconia mill with a single ball of 5 cm diameter) for 1 h. The mixture was calcined for 6 h at 1100 °C in air, largely decomposing the $BaCO_3$ but not completely forming the $BaZrO_3$ perovskite phase. Then, 0.5 wt.% NiO (Alfa Aesar) was added and the powder was milled for 24 h in a planetary mill (Fritsch Pulverisette 5, 200 rpm, ca. 30 g powder with 12 zirconia balls in a zirconia vial with 50 mL 2-propanol). After drying, the powders received a final 1 h dry ball milling and were pressed isostatically into pellets. The pellets were sintered for 16 h at 1550 °C in air (heating rate

300 K min^{-1}, cooling rate 150 K min^{-1}) in YSZ crucibles, covered with excess $BaZrO_3$ powder (Sigma Aldrich) to prevent BaO loss.

The samples were hydrated in a pure steam atmosphere ($pH_2O = 1$ bar) in a quartz setup inserted with a slight inclination into a tube furnace. The steam was generated by water slowly pumped with a peristaltic pump towards the hot zone where it evaporated; excess water condensed at the air-cooled gas outlet. The temperature was lowered stepwise (6 h at 750 °C, 18 h at 700 °C, 24 h at 650 °C, 48 h at 600 °C, 96 h at 550 °C) to achieve a high degree of hydration.

XRD patterns of the ceramic pellets were acquired (TTrax Rigaku diffractometer in Bragg Brentano Θ/2Θ mode, 2° min^{-1}), and the lattice parameters were calculated (MDI Jade 2010 software).[38] The SEM images of the top surface of the ceramic pellets were acquired (Sigma FEG, Zeiss, 3kV accelerating voltage) after surface etching in 10% HCl solution. The grain size of each sample was calculated by averaging the measurement of 20 grains. The M_{33} electrostriction coefficient was calculated from the change in sample dimensions parallel to the direction of the applied electric field. This change was measured using a custom-made setup based on a capacitive proximity sensor (Lion Precision, CPL190) described in ref. [2]. An alternating voltage was applied by a function generator (Keithley, 3390) and amplified (Trek, 610E) to reach amplitudes of 500–900V within frequency range 0.25–3000 Hz. Voltage amplitudes of 250–2750 V and a frequency of 0.15 Hz were used for strain saturation measurements. The second harmonic signal from the proximity sensor was averaged by a dual-phase lock-in amplifier (Signal Recovery, 7265). The signal was recorded and processed with a Matlab-written code. Three measurements were performed for each voltage (nine measurements for each sample) to ensure reproducibility and the calculated coefficient was averaged.

The metric density of samples was determined by the Archimedes method with ethanol as a liquid medium. The mechanical integrity of the samples was verified by observing ultrasound pulse-echo decay using a USN 60L transducer (GE Inspection Technologies). Only the samples with at least ten reflections, indicating the absence of cracks and fissures, were used for this study. USTOF was used to measure the unrelaxed longitudinal and transversal sound velocities, from which the unrelaxed Young's modulus (Y) of the ceramics was deduced.[14]

Supporting Information

Supporting Information is available from the Wiley Online Library or from the author.

Acknowledgements

The authors thank Y. Huang (powder preparation), H. Hoier (XRD), crystal preparation group (cutting and polishing of samples), and E. A. Kotomin and M. Hoedl (numerous valuable discussions), all from the Max Planck Institute for Solid State Research Stuttgart. This work was funded by the German Israeli Foundation (project I-1342-302.5/2016) and in part by the BioWings project, which has received funding from the European Union's Horizon 2020 under the Future and Emerging Technologies (FET) program with grant agreement No. 801267.

Conflict of Interest

The authors declare no conflict of interest.

Data Availability Statement

The data that support the findings of this study are available from the corresponding author upon reasonable request.

Keywords

elastic-dipoles, electrostriction, point defects, proton conductors

Received: May 3, 2021
Revised: August 13, 2021
Published online: September 12, 2021

[1] R. E. Newnham, V. Sundar, R. Yimnirun, J. Su, Q. M. Zhang, *J. Phys. Chem. B* **1997**, *101*, 10141.
[2] N. Yavo, A. D. Smith, O. Yeheskel, S. R. Cohen, R. Korobko, E. Wachtel, P. R. Slater, I. Lubomirsky, *Adv. Funct. Mater.* **2016**, *26*, 1138.
[3] R. Korobko, A. Lerner, Y. Y. Li, E. Wachtel, A. I. Frenkel, I. Lubomirsky, *Appl. Phys. Lett.* **2015**, *106*, 042904.
[4] R. Korobko, A. Patlolla, A. Kossoy, E. Wachtel, H. L. Tuller, A. I. Frenkel, I. Lubomirsky, *Adv. Mater.* **2012**, *24*, 5857.
[5] Y. Y. Li, O. Kraynis, J. Kas, T. C. Weng, D. Sokaras, R. Zacharowicz, I. Lubomirsky, A. I. Frenkel, *AIP Adv.* **2016**, *6*, 055320.
[6] N. Yavo, O. Yeheskel, E. Wachtel, D. Ehre, A. I. Frenkel, I. Lubomirsky, *Acta Mater.* **2018**, *144*, 411.
[7] M. Hadad, H. Ashraf, G. Mohanty, C. Sandu, P. Muralt, *Acta Mater.* **2016**, *118*, 1.
[8] A. Kabir, H. W. Zhang, S. Colding-Jorgensen, S. Santucci, S. Molin, V. Esposito, *Scr. Mater.* **2020**, *187*, 183.
[9] A. Kabir, M. Espineira-Cachaza, E. M. Fiordaliso, D. Y. Ke, S. Grasso, B. Merle, V. Esposito, *J. Eur. Ceram. Soc.* **2020**, *40*, 5612.
[10] E. Wachtel, A. I. Frenkel, I. Lubomirsky, *Adv. Mater.* **2018**, *30*, e1707455.
[11] M. Varenik, J. C. Nino, E. J. Wachtel, S. Kim, O. Yeheskel, N. Yavo, I. Lubomirsky, *ACS Appl. Mater. Interfaces* **2020**, *12*, 39381.
[12] K. D. Kreuer, *Annu. Rev. Mater. Res.* **2003**, *33*, 333.
[13] M. F. Hoedl, E. Makagon, I. Lubomirsky, R. Merkle, E. A. Kotomin, J. Maier, *Acta Mater.* **2018**, *160*, 247.
[14] E. Makagon, R. Merkle, J. Maier, I. Lubomirsky, *Solid State Ionics* **2020**, *344*, 115130.
[15] T. Scherban, A. S. Nowick, *Solid State Ionics* **1989**, *35*, 189.
[16] T. Matzke, U. Stimming, C. Karmonik, M. Soetratmo, R. Hempelmann, F. Guthoff, *Solid State Ionics* **1996**, *86–8*, 621.
[17] K.-D. Kreuer, W. Muench, M. Ise, T. He, A. Fuchs, U. Traub, J. Maier, *Ber. Bunsenges. Phys. Chem.* **1997**, *101*, 1344.
[18] R. Hempelmann, M. Soetratmo, O. Hartmann, R. Wappling, *Solid State Ionics* **1998**, *107*, 269.
[19] R. A. Davies, M. S. Islam, J. D. Gale, *Solid State Ionics* **1999**, *126*, 323.
[20] M. E. Bjorketun, P. G. Sundell, G. Wahnstrom, *Phys. Rev. B* **2007**, *76*, 054307.
[21] S. J. Stokes, M. S. Islam, *J. Mater. Chem.* **2010**, *20*, 6258.
[22] Y. Yamazaki, F. Blanc, Y. Okuyama, L. Buannic, J. C. Lucio-Vega, C. P. Grey, S. M. Haile, *Nat. Mater.* **2013**, *12*, 647.
[23] Y. Yamazaki, A. Kuwabara, J. Hyodo, Y. Okuyama, C. A. J. Fisher, S. M. Haile, *Chem. Mater.* **2020**, *32*, 7292.
[24] A. Fluri, A. Marcolongo, V. Roddatis, A. Wokaun, D. Pergolesi, N. Marzari, T. Lippert, *Adv. Sci.* **2017**, *4*, 1700467.
[25] F. M. Draber, C. Ader, J. P. Arnold, S. Eisele, S. Grieshammer, S. Yamaguchi, M. Martin, *Nat. Mater.* **2020**, *19*, 577.
[26] R. D. Shannon, *Acta Crystallogr. A* **1976**, *32*, 751.
[27] J. Wu, R. A. Davies, M. S. Islam, S. M. Haile, *Chem. Mater.* **2005**, *17*, 846.
[28] D. L. Han, Y. Nose, K. Shinoda, T. Uda, *Solid State Ionics* **2012**, *213*, 2.
[29] D. L. Han, K. Kishida, K. Shinoda, H. Inui, T. Uda, *J. Mater. Chem. A* **2013**, *1*, 3027.

[30] M. Varenik, J. C. Nino, E. Wachtel, S. Kim, S. R. Cohen, I. Lubomirsky, *ACS Appl. Mater. Interfaces* **2021**, *13*, 20269.
[31] E. Jedvik, A. Lindman, M. P. Benediktsson, G. Wahnstrom, *Solid State Ionics* **2015**, *275*, 2.
[32] E. Gilardi, E. Fabbri, L. Bi, J. L. M. Rupp, T. Lippert, D. Pergolesi, E. Traversa, *J. Phys. Chem. C* **2017**, *121*, 9739.
[33] E. Bevillon, J. Hermet, G. Dezanneau, G. Geneste, *J. Mater. Chem. A* **2014**, *2*, 460.
[34] A. Loken, T. S. Bjorheim, R. Haugsrud, *J. Mater. Chem. A* **2015**, *3*, 23289.
[35] A. S. Nowick, B. S. Berry, *Anelastic relaxation in crystalline solids*, Academic Press, New York **1972**.
[36] T. Das, J. D. Nicholas, B. W. Sheldon, Y. Qi, *Phys. Chem. Chem. Phys.* **2018**, *20*, 15293.
[37] Y. Huang, R. Merkle, J. Maier, *Solid State Ionics* **2020**, *347*, 115256.
[38] N. A. Razik, *Appl. Phys. A: Mater. Sci. Process.* **1985**, *37*, 187.
[39] I. Levin, T. G. Amos, S. M. Bell, L. Farber, T. A. Vanderah, R. S. Roth, B. H. Toby, *J. Solid State Chem.* **2003**, *175*, 170.
[40] S. Yamanaka, M. Fujikane, T. Hamaguchi, H. Muta, T. Oyama, T. Matsuda, S. I. Kobayashi, K. Kurosaki, *J. Alloys Compd.* **2003**, *359*, 109.